JOURNAL OF THERMOPHYSICS AND HEAT TRANSFER
Vol. 24, No. 1, January–March 2010

Nonequilibrium Radiation in Shocked Martian Mixtures

Pascal Boubert*
Université de Rouen, 76800 Saint-Etienne-du-Rouvray, France
and
Catherine Rond†
Université Paris 13, 93430 Villetaneuse, France

DOI: 10.2514/1.45385

Shock-tube experiments are carried out to study the radiation emitted during a vehicle entry in the Mars atmosphere. CN and C_2 emission absolute intensity measurements are performed behind a strong shock wave in a CO–N_2 mixture with two different conditions of initial pressure and velocity. The CN violet system bands are shown to be self-absorbed. Temperatures and CN mole fractions are derived using this phenomenon in the nonequilibrium part of the shocked gas. C_2 absolute emission intensities are measured in different mixtures: CO–N_2, CO_2–N_2, and pure CO_2. Some comparisons with two-temperature calculations are presented. Such a two-temperature model fails to correctly reproduce CN and C_2 experimental radiative flux densities but is suitable for mole fraction predictions.

Nomenclature

A	=	reaction rate constant
k_f	=	forward reaction rate
p_i	=	initial pressure in the shock tube
p_s	=	postshock pressure
T_a	=	geometrical average of kinetic and vibrational temperatures, $\sqrt{T_k.T_{\text{vib}}}$
T_d	=	reaction characteristic temperature
T_{eq}	=	equilibrium temperature
T_k	=	kinetic temperature
T_{vib}	=	vibrational temperature
t	=	laboratory time
v_s	=	shock velocity
X_{C2}	=	molar fraction of C_2 molecule
X_{CN}	=	molar fraction of CN molecule
X_{CO}	=	molar fraction of CO molecule
Δv	=	difference between the upper and lower vibrational levels of a radiative transition

I. Introduction

FUTURE exploration missions toward the planet Mars will require further understanding of physical and chemical processes occurring during the probe entry in the upper atmosphere. As shown in Table 1, past spacecraft were quite light and the entry velocities remained moderate. So the resulting peak heat fluxes and total heat loads were sustainable for ablative materials. Moreover, in these conditions, the radiative heat flux only represented a few percent of the total heat flux. In fact, for stagnation pressures lower than 2×10^4 Pa, low-density thermal protection systems (TPS) such as SLA-561 used on those spacecraft are still suitable [1].

The entry velocity of the vehicle in projected missions is higher than 7 km/s. The next spacecraft will be heavier and will encounter a very large convective as well as radiative heat load. The estimate of the radiative flux on the spacecraft wall needs to be improved to increase the confidence in new TPS and the relative mass of the scientific payload.

The interaction between a plasma flow and a surface can be reproduced in a plasma wind tunnel (arcjet [2], inductively coupled plasma [3]), but the physical and chemical conditions behind an entry shock wave can only be obtained thanks to a shock tube. Although plasma wind tunnels can be operated for hours, the effective test time behind a shock front moving at a few kilometers per second is in the order of few microseconds. Just behind the shock front, the pressure jump induces a high kinetic temperature but the energy exchange characteristic times are too small to ensure equilibrium. Physical and chemical processes occurring in this zone should then be considered as out of equilibrium.

Shock-tube experiments have been used for a long time to study shock waves in mixtures containing carbon dioxide. Some of these studies focus on a Venusian application with pure CO_2 gas. For example, the C_2 Swan and CO fourth positive systems were observed by Nealy and Haggard [4] and Nealy [5]. The very valuable experiments by Thomas and Menard [6], who carried out radiative flux measurements at various wavelengths in different CO_2–N_2 mixtures and in pure CO_2, also have to be cited. Gorelov et al. [7] provided the relaxation of electronic temperature and density for a mixture close to the actual Martian atmosphere composition with an initial pressure equal to 26.6 Pa and shock velocities from 4 to 8.5 km/s. At the same time, Losev et al. [8] carried out time-resolved emission measurements in CO_2–N_2 mixtures highly diluted in argon for velocities lower than 3.75 km/s and initial pressures of about 100 Pa.

Different groups using different kinds of shock tubes recently published some relevant results concerning radiation behind a strong shock wave in mixtures related to Mars and Titan atmospheres. Indeed, because of the high CN and C_2 radiation, experiments on Titan mixture plasmas are also very interesting as complementary test cases.

Experiments were carried out in the NASA Ames Research Center Electric Arc Shock Tube at high velocities and low pressures with various N_2–CH_4 mixtures [9] and with a 96% CO_2–4% N_2 mixture [10,11] (thereafter, all mixture compositions will be given as volume fractions). Those last results consist in emission spectroscopy measurements of the CN violet systems, C_2 Swan bands, and atomic lines as well as the first quantitative measurement of the CO fourth positive system in such conditions.

In parallel, some tests were realized at the University of Provence on the TCM2 free-piston shock tube with various N_2–CH_4–Ar mixtures related to the expected composition of the Titan atmosphere (before Huygens successful mission) [12] and a 70% CO_2—30% N_2 mixture [13]. The latter tests highlighted discrepancies in the

Received 11 May 2009; revision received 12 October 2009; accepted for publication 25 October 2009.

*Assistant Professor, Department of Physics, Plasma Group, Complexe de Recherches Interprofessionnel en Aérothermochimie, Boîte Postale 12; boubert@coria.fr.

†Assistant Professor, Department of Plasma Processing for Materials Elaboration, Laboratoire d'Ingénierie des Matériaux et des Hautes Pressions, 99 Avenue Jean-Baptiste Clément; rond@limhp.univ-paris13.fr.

Table 1 Characteristics of some Martian spacecraft atmospheric entries [27]

Spacecraft	Year	Mass, kg	Entry velocity, km/s	Peak heat flux density, MW/m^2	Total heat load density, MJ/m^2
Viking	1976	992	4.7	0.26	11
Mars Exploration Rover	2004	830	5.5	0.44	36.87
Phoenix	2008	600	5.67	0.58	32.45
Mars Pathfinder	1997	584	7.26	1.00	39
Mars Science Laboratory	2011	2800	6	1.55	<60

rebuilding of the CN radiation temporal profiles because of the uncertain CO_2 dissociation rate from commonly used models.

More recently, Anokhin et al. [14] published some results obtained at the Moscow Institute of Physics and Technology in a hydrogen–oxygen–helium combustion shock tube with a 70% CO and 30% N_2 mixture with shock velocities ranging from 4 to 6.5 km/s and with initial test gas pressures between 175 and 1100 Pa. They gave temporal profiles of the CN violet and red systems and C_2 Swan bands. Even more recently, the same authors performed experiments on pure CO_2 mixtures to measure CO_2 dissociation and electron density.[‡] They had previously investigated the emission of CO_2–N_2–Ar plasmas with various dilution ratios in argon [15].

Lee et al. [16] used a static high hydrogen pressure shock tube with a 78% CO—22% N_2 mixture at the Korean Advanced Institute of Science and Technology. These experiments were carried out in reflected shock conditions in which the equivalent shock velocity reached 5 km/s and the equivalent driven gas pressure was between 500 and 1100 Pa. The measured temporal profiles of the CN violet main vibrational manifolds were compared with model results.

Finally, CN radiation was also recently measured at the exit of the X2 free-piston shock tube at the University of Queensland in Australia by Brandis et al. [17] for a wide range of velocity, pressure, and composition conditions.

As shown, the radiative flux has been widely investigated through optical emission spectroscopy until now. However, the physical and chemical models still have to be validated. Then many experimental data are required to question them. One of the main points is the fact that radiation is due to excited states whereas the classical models deal with nonexcited species. Consequently, opportunities to get data about radiative fluxes of main radiators, temperatures, and densities together behind a strong shock wave in Martian mixtures should be seized. To correctly predict the radiation of molecules such as CO, CN, and C_2, the estimate of CO_2 dissociation also has to be improved.

This paper presents results of CN spontaneous emission behind a shock wave for a mixture of carbon monoxide and nitrogen for two running conditions with absolute intensity, mole fraction, and temperature temporal profiles. C_2 quantitative radiative heat flux densities are also presented for one of the previous running conditions in pure CO_2 and in CO–N_2 and CO_2–N_2 mixtures. Some comparisons with a two-temperature model are also exposed to highlight the limit of such a calculation.

II. Facility and Instrumentation

A. Shock-Tube Facility

The experimental investigations were carried out in a shock-tube facility known as TCM2, located at the University of Provence in Marseille, France. TCM2 was initially built as a powerful and clean wind tunnel for testing in air. It has been modified to work as a shock tube with mixtures such as N_2–CH_4–Ar, CO–N_2, CO_2–N_2, and pure gases. This facility works according to the Stalker principle: a free piston (35 kg) hurled by high-pressure air continuously and adiabatically compresses a mass of helium used as a driver gas. When the pressure in the helium reaches a critical value, a steel membrane (2 mm thick) bursts and compression waves converge to a shock wave along the shock tube where the test gas is at rest. Figure 1 gives an overview of the facility with useful dimensional details. An extensive description of this facility and its functioning is given in [18,19].

The internal diameter of the stainless steel shock tube is 70 mm. It is equipped with four pressure transducers that allow the shock front during a run to be located and then the shock velocity to be measured. Between two runs, both compression and shock tube are evacuated to a pressure of a few hundredths of a pascal by a primary-root pump system. A stainless steel chamber is located 6 m after the main membrane and is equipped on both sides with two 25 mm quartz windows to carry out optical measurements inside the shock tube.

B. Working Conditions

Some previous experiments were carried out with a mixture of 70% CO_2 and 30% N_2 [13]. They revealed a two-phase temporal profile of the CN emission and a very low vibrational temperature for the $B^2\Sigma^+$ excited state of CN. During those previous experiments, the pressure was about 200 Pa and the shock velocity was close to 6.2 km/s. For the present study, the mixture is made up of carbon monoxide and nitrogen in the same C/N ratio as in the previous study (70% CO and 30% N_2). Despite the difference from the actual composition of the Martian atmosphere, such a ratio allows the emission signal-to-noise-ratio to be significantly improved whereas the chemical kinetics processes remain the same. Two initial pressure/shock velocity conditions were studied: $p_i = 320$ Pa and $v_s = 6.2$ km/s (called the moderate-pressure condition), and $p_i = 45$ Pa and $v_s = 6.9$ km/s (called the low-pressure condition). For these conditions, CN violet ($B^2\Sigma^+ \rightarrow X^2\Sigma^+$) and C_2 Swan ($d^3\Pi_g \rightarrow a^3\Pi_u$) emissions were monitored. Some complementary experiments were also carried out in the low-pressure condition with a 70%CO_2–30%C_2 mixture and also pure CO_2 monitoring the C_2 Swan emission (Table 2).

The relative uncertainties of the mixture compositions are lower than 2%. Moreover, the contamination of the test mixture by outside air can be neglected because of the weak leakage rate of the shock tube. It was reduced in comparison to previous studies to a value always lower than 0.01 Pa/ min. Moreover, before each new filling, the shock tube was flushed several times with the next test gas and then pumped again. The initial pressure in the shock tube is known with an accuracy of 1 Pa but varies shot-to-shot. Tests were carried out with pressures ranging between 42 and 47 Pa for the low-pressure condition and between 315 and 325 Pa for the moderate-pressure condition. The corresponding shock velocities ranged, respectively, between 6.76 and 6.92 km/s and between 6.21 and 6.27 km/s. There is no obvious correlation between the variations of the initial pressure and the variations of the shock velocity because some others parameters are involved, such as the air pressure in the high-pressure chamber when the membranes burst.

Table 2 Working conditions: pressure, shock velocity, and mixtures

Conditions	Pressure, Pa	Shock velocity, km/s	Mixtures
Low pressure	45	6.9	70% CO–30% N_2 70% CO_2–30% N_2 100% CO_2
Moderate pressure	320	6.2	70% CO–30% N_2

[‡]Private communication with A. Starikovskii, March 2008.

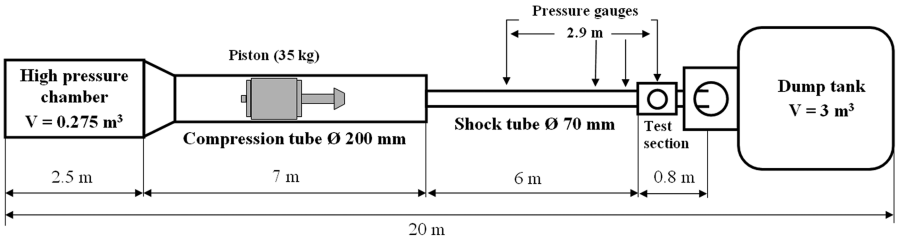

Fig. 1 TCM2 shock-tube geometry and characteristics.

C. Shock Velocity Measurements

Four dynamic pressure gauges are placed above the center point of the optical section and 750, 1150, and 2900 mm upstream from this point. The shock velocity is estimated from the gauge signal recordings on a four-channel digitizing oscilloscope and by detecting the shock front using a homemade electronic processor. This device calculates the velocity of the shock wave in the driven tube and predicts its arrival time in front of the test section to trigger the optical measurement channel. The velocities measured by both systems are in very good agreement. The size of the transducer effective surface induces an uncertainty on the shock velocity measurement that remains lower than 40 m/s (relative uncertainty: 0.7%) whatever the experimental conditions.

D. Calibrated Time-Resolved Emission Spectroscopy

The short duration of a run in a shock tube (about 20 μs for our experiments) compels the use of diagnostic techniques providing a lot of data. As mentioned earlier, our experiments are aimed to get information about radiation flux on the one hand, and chemical kinetics in the plasma on the other hand. The former needs absolute measurements whereas the latter needs the monitoring of temperatures and densities with a sufficient temporal resolution. Spontaneous emission brings some information about the excited radiative levels, mainly density and temperatures. Thanks to assumptions on collisional time scales and self-absorption, the obtained values may be connected to ground-state values. Actually, for pressures larger than a few hundred pascals, the translation temperature is often very representative of the rotational distribution of molecular excited states. The vibrational temperature is also generally supposed to be the same whatever the considered state of a same species. However, the coupling of the vibration with a possible electronic temperature should be questioned.

Experiments can be carried out either by recording the radiation coming from the whole space around the shock front or by temporally following the radiation emitted from a small fixed volume crossed by the shock wave. The evolutions derived from both methods may be easily compared. Within this study, time-resolved emission spectroscopy was used in near-ultraviolet and visible ranges and the results behind the shock wave are presented as temporal profiles.

A Jobin–Yvon HR640 monochromator was used with a 1200 lines/mm grating suitable for measurements from 370 to 560 nm (Fig. 2). The entrance slit was fixed at 200 μm to get an acceptable signal-to-noise ratio and a sufficient spectral resolution. The latter also depends on the size on the charged coupled device's (CCD) pixels. On all the spectra extracted, the spectral resolution is equal to 0.5 nm, which allows the vibrational bands to be distinguished. A time-spectral image is provided by coupling a streak unit (Hamamatsu M1953) with the monochromator used as a flat field spectrograph. The resulting light dispersion was recorded on a CCD array (Hamamatsu C1587). An example of the recording is shown in Fig. 3.

To obtain both a temporal resolution that captures the nonequilibrium part of the radiation behind the shock front and a good signal-to-noise ratio, the light was collected through a 500 μm vertical slit located just behind the fused-silica windows of the shock tube. That slit was also used to avoid unexpected reflected light. Two time ranges were used within this study, 20 and 200 μs, corresponding to temporal resolution equal to 0.3 and 1.5 μs, respectively. To reduce the background noise and avoid the fatigue phenomenon, the CCD detector was active only during the acquisition time.

The optical collection setup was composed by two achromatic doublets that allowed a large depth of field on a wide range of wavelengths. Unfortunately, that setup prevented some measurements to be carried out for wavelengths lower than 370 nm. The setup remained unchanged during the calibration process and was calibrated by using a tungsten halogen lamp (Heraeus LSB021) working with a current intensity equal to 6.6 A. This lamp had been itself calibrated by the manufacturer against two lamps certified by the National Physical Laboratory in Great Britain and the Physikalisch-Technische Bundesanstalt in Germany, respectively. Some calculations (described in [12]) were carried out to identify the volume of collection. Moreover, several acquisitions with the tungsten lamp were performed along the optical path to validate those calculations. Because of the difference in spectral radiances between the calibration lamp and the plasma, different time ranges and

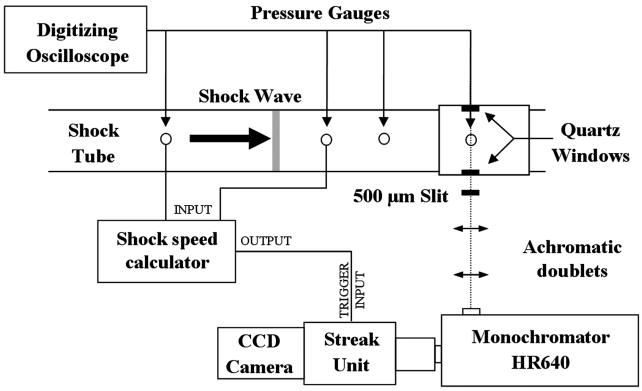

Fig. 2 Time-resolved emission spectroscopy optical setup.

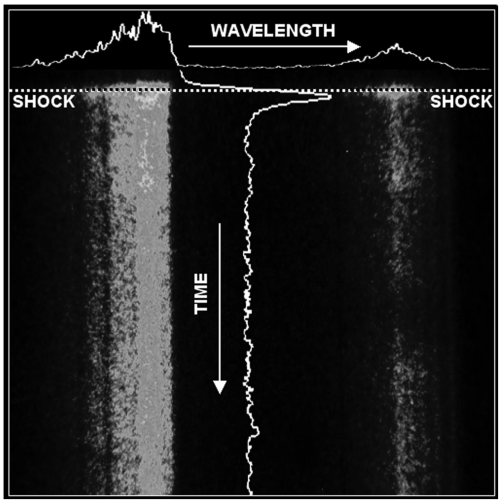

Fig. 3 Time-spectral image of CN violet $\Delta v = 0$ and -1. The wavelength range is 383–391 nm and the time gate width is 20 μs.

amplification factors were used. The corresponding corrections were determined experimentally. Finally, the light received by each pixel of the CCD array during a test was calibrated and the value was introduced in postprocessing to derive temporal and spectral profiles. Considering each specific uncertainty in the calibration process, the total uncertainty on the calibration process has been estimated to be ±19%.

E. Optical Measurements in a Moving Shock Tube: Reproducibility

TCM2 was built as a wind tunnel and the first measurements were carried out above a model at the exit of a nozzle [19]. The Stalker system generates a recoil of the facility that induces a displacement of the shock tube during the tests. During previous experiments, light used to be collected through a fiber optics that was strongly connected with the tube and moved with it. However, past experiments [12] showed that the amount of collected light in the same initial conditions varied from one run to another. Thus, fiber optics presented two main issues to be addressed: reproducibility of the run and light loss by absorption on a long path.

Then investigations were carried out to monitor the displacement timing of the shock tube and to locate the optical axis when the shock wave passed in front of the windows. Those runs highlighted that the recoil of the tube was not very sensitive to the initial pressure inside. Furthermore, the total recoil of the tube had a very high reproducibility for runs with similar high-pressure chamber and driver tube conditions.

By exposing a classic digital camera to the light emitted behind the shock wave, the position of the shock tube when the shock wave was in front of the center of the windows was determined with an accuracy of lower than 1 mm. The reproducibility was excellent. It was then possible to predict the position of the shock tube at the measurement time and then to set the position of the tube before the run out of the optical axis. Within this study, whatever the gas test and the initial conditions, the shock-tube position was set 32.5 mm ahead of the optical axis. The position of the tube at the end of the experiments was observed to be between 8 and 10 mm ahead of the optical axis (the tube moves forward, then goes back during a run).

No experiment was performed with either the fiber optics setup or the new setup, but comparisons between similar experiments allowed an increase close to 400% in terms of intensity to be estimated. Previous estimates [12] showed that run-to-run variations with the fiber optics setup were about 25%. The tests made within this study are close to each other: for the total amount of light collected as well as for the time and spectral evolutions, the run-to-run variations are lower than 5%. For example, Fig. 4 presents the time and spectral absolute profiles of C_2 Swan emission for two experiments in close conditions. To evaluate the reproducibility, five successive runs were carried out with those conditions. The two sets of plots in Fig. 4 represent the two most different results. Considering the uncertainty on calibration and the shot-to-shot reproducibility, it can be considered that the absolute intensities are known as near as ±23%.

F. Postprocessing and Spectral Calculations

Time-spectral images were numerically processed to extract spectra at different moments behind the shock front on the one hand, and temporal profiles of vibrational manifolds or individual bands on the other hand. The code sums the intensity received by each pixel over several lines and smooths the time (respectively, spectral) evolutions obtained with regard to the time (respectively, spectral) resolutions. Taking into account those resolutions and convolution functions, it was also possible to deconvolute the extracted temporal profiles to obtain some results directly comparable with chemical kinetic calculations. Experimental and calculated spectra were then compared to estimate free parameters of the calculations (temperatures and densities). The calculated spectra are produced by a spectral simulation code called PASTIS [20]. Spectroscopic parameters for the CN violet system and C_2 Swan bands can be found in [12]. Derivation of temperatures and densities was carried out by a least mean square method. A multistep accuracy approach was used to avoid multiple solutions when several free parameters were used and to increase the accuracy as well as the calculation time. In this method, best parameters were determined with an accuracy that increases with iterations.

III. Results for CN: $CO–N_2$ Mixture

A. Self-Absorption

Radiative calculations carried out in optically thick conditions suggest that the CN mole fraction significantly influences both the absolute intensity and relative shape of the spectrum. The comparison between experimental spectra and calculations in optically thin conditions confirms that self-absorption plays a determining role in CN radiation.

Moreover, self-absorption allows access to the CN ground-state density. The absolute intensity and relative shape of the CN violet three main manifolds are actually very sensitive to the CN density in the case of an emission along a homogeneous media 70 mm long (internal diameter of the shock tube). For example, Fig. 5a shows their evolution for three different molar fractions at a fixed pressure and equilibrium temperature (6400 K). An increase of the CN molar fraction by a factor of 10 (0.15–1.5%) induces an increase of the $\Delta v = -1$ vibrational manifold (417 nm) total radiance by a factor equal to 7.5, suggesting a low self-absorption. On the other hand, the $\Delta v = 0$ vibrational manifold (390 nm) total radiance only increases by a factor of close to 3, which suggests a significant self-absorption. When the CN molar fraction is multiplied by 10 again (1.5–15%), the total radiance increases are equal to 3.2 and 1.8 for $\Delta v = -1$ and $\Delta v = 0$ vibrational manifolds, respectively. The evolution of the

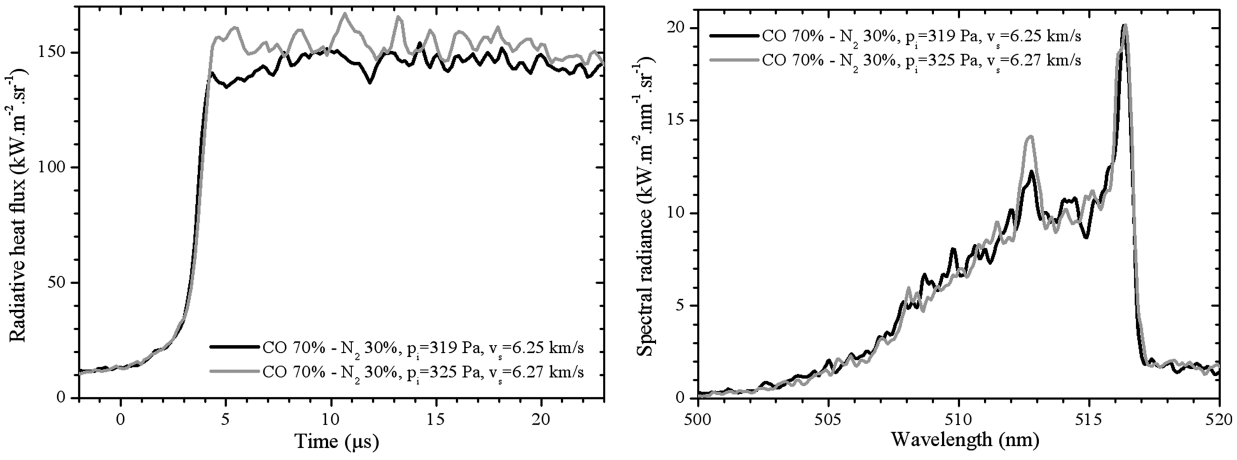

a) b)

Fig. 4 Absolute radiative emission (C_2 Swan $\Delta v = 0$) for two runs in similar conditions (moderate pressure): a) time, and b) wavelength.

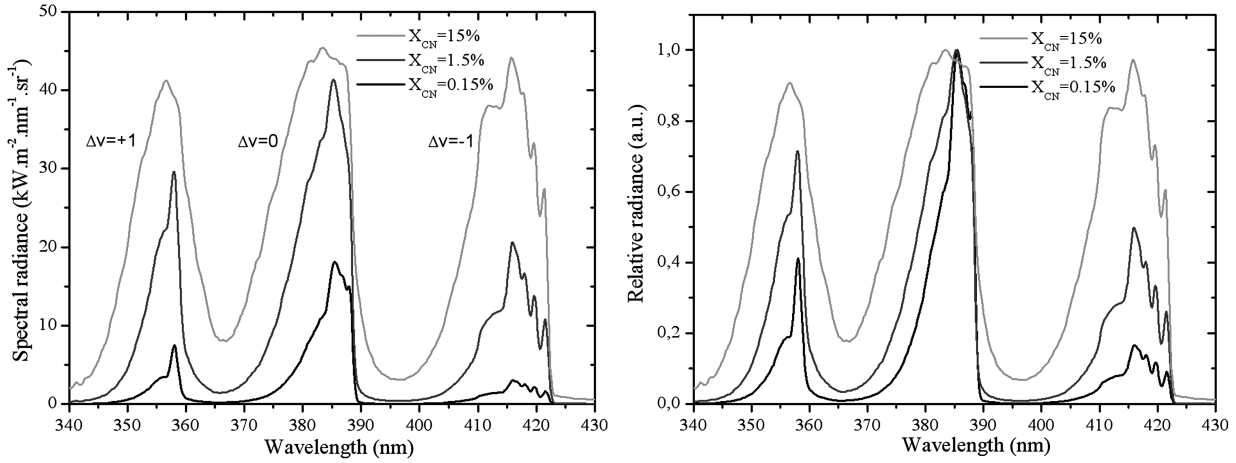

a) b)

Fig. 5 Effect of self-absorption. Evolution of CN violet spectrum with CN mole fraction: a) absolute, and b) relative. The equilibrium temperature is $T_{eq} = 6400$ K.

ratio between both vibrational manifolds is clearly visible by normalizing the previous spectrum (Fig. 5b).

Further data can be obtained from the study of the CN violet spectrum when self-absorption is sufficient. Actually, this spectrum is also very sensitive to the vibrational temperature as shown in Fig. 6a, which presents the normalized spectrum of the CN violet main manifolds for a fixed CN mole fraction equal to 1.5% and three different vibrational temperatures (the electronic temperature is kept equal to 6400 K). The vibrational temperature here is supposed to be the same for both the $B^2\Sigma^+$ excited state and $X^2\Sigma^+$ ground state. This hypothesis is validated by the good correlation between the measured vibrational temperatures of the excited states and the electronic temperature. Some calculations carried out with the electronic temperature as a free parameter proved that better agreement with the experiments was achieved when it was quite equal to the vibrational temperature.

There is a clear influence of the vibrational temperature on the shape of the $\Delta v = -1$ vibrational manifold even at low resolution. Notice, moreover, that the intensity of the $\Delta v = +1$ vibrational manifold (355 nm) is also very sensitive to the vibrational temperature because it does not imply the vibrational ground state of the $B^2\Sigma^+$ electronic state. Unfortunately, that manifold was not captured because of the limitations of the optical setup.

As an illustration, some calculations were carried out to reproduce CN experimental spectra obtained by Lee et al. [16] and Anokhin et al. [14]. The comparison between a calculated spectrum and the relative values of the peaks of the vibrational manifolds obtained by both groups of authors is plotted in Fig. 6b (the normalization has been done on the peak of the $\Delta v = 0$ vibrational manifold). Relative intensities are correctly reproduced in both cases using vibrational and electronic temperatures (2800 K) much lower than the equilibrium temperature (6100 K). Such a departure had been already observed in experiments at the TCM2 facility [13]. Nevertheless, the experimental CN spectrum presented in [16] does not agree with such a low vibrational temperature, suggesting a difference between the vibrational and electronic temperatures (those temperatures are considered to be equal in our calculations).

Therefore, self-absorption must be taken into account in such conditions. It is a powerful tool to get more data from emission measurements in shock tubes because it makes spectra much more sensitive to parameters such as vibrational temperature and, of course, ground-state density. In our analyses, we assumed that densities are constant along the optical path, which involves neglecting the boundary layer on the wall of the tube. This assumption has to be addressed by computational fluid dynamics, but good agreement between experimental and calculated values at equilibrium for most cases suggests that the influence of the boundary layer is weak.

B. Experimental Results

We chose to work under low spectral resolution (0.5 nm) to limit the number of tests and to be able to capture the near-ultraviolet and visible spectrum from 370 to 540 nm with three runs. As expected in

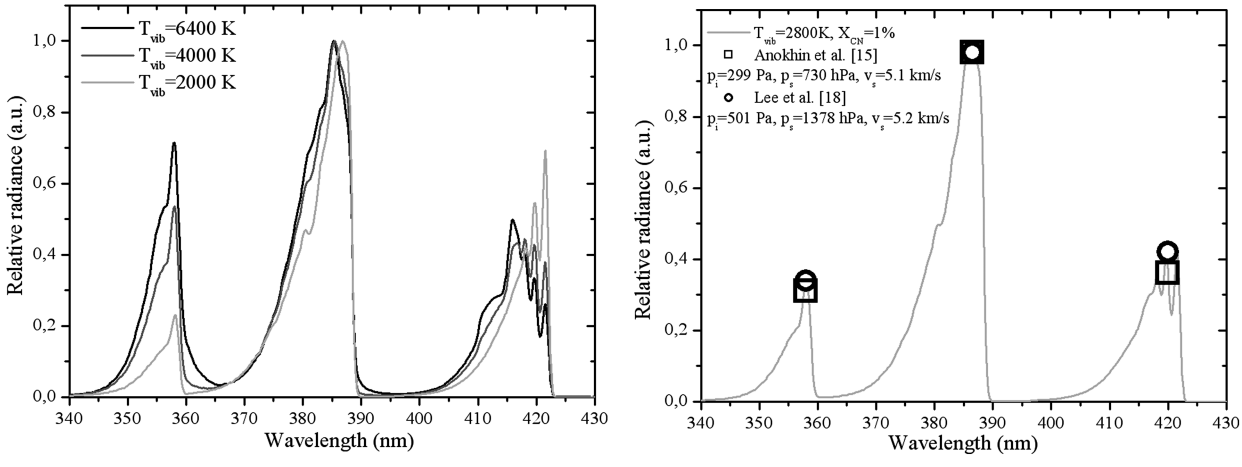

a) b)

Fig. 6 Effect of self-absorption: a) evolution of CN violet spectrum with the vibrational temperature, and b) comparison between our calculation and results from Lee et al. [16] and Anokhin et al. [14].

that spectral range, the CN violet system and C_2 Swan bands clearly dominate the spectrum (Fig. 7). Attempts to point out a measurable emission from the CO Angström system or CO triplet systems (triplet, Asundi, Herman) remained unsuccessful.

All the experimental spectra were compared with calculations (PASTIS code) to estimate the internal mode temperatures. A comparison between an equilibrium spectrum corresponding to the moderate-pressure condition and a calculation is shown in Fig. 7. The good agreement corresponds to an equilibrium temperature $T_{eq} = 6400 \pm 400$ K and to the following molar fractions, $X_{CN} = 8.4 \pm 0.5 \times 10^{-3}$, $X_{C2} = 3.7 \pm 0.3 \times 10^{-4}$, and $X_{CO} = 0.43$, with a postshock pressure equal to 1.26×10^5 Pa. The CO mole fraction and the postshock pressure are calculated values at equilibrium.

Considering the diameter of the shock tube (70 mm) as well as the initial test gas pressure, the shock front duration may be estimated as close to 0.13 μs for an initial pressure equal to 320 Pa and close to 0.3 μs for an initial pressure equal to 45 Pa. In the latter case, experimental spectra are averaged over 0.3 μs in the nonequilibrium part and over 1 μs in the equilibrium part. Comparisons between these spectra and the calculated ones allow the temporal profile of CN molar fractions and temperatures to be drawn. Figure 8 presents these experimental temporal profiles for the low-pressure conditions, wherein each point was obtained by the simulation of the average experimental spectra. It is assumed that the electronic temperature is equal to the vibrational temperature. In the first microseconds after the shock front, the electronic and rotational temperatures can be distinguished with an increase of the first one and a decrease of the second one. The average uncertainty on the temperatures is about 1000 K but it rises up to 1500 K in the first microsecond. The absolute uncertainty on the CN molar fraction is mainly connected to the uncertainty on the temperatures. Considering the sensitivity of the method, it is estimated to be not less than $\pm 10^{-2}$ for the four first points and $\pm 5 \times 10^{-3}$ up to 7 μs. When equilibrium is reached, the uncertainty is then much better and is close to 5×10^{-4}.

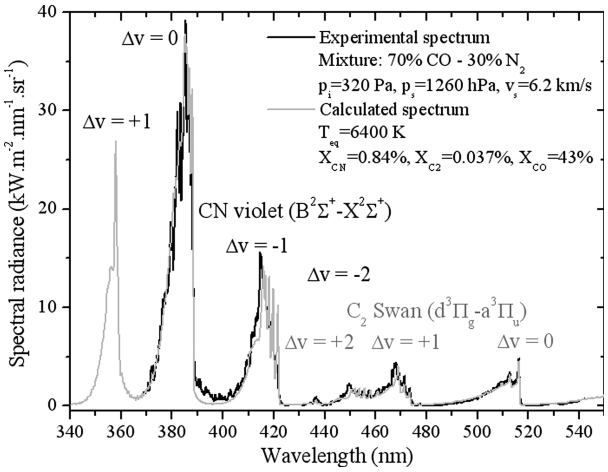

Fig. 7 Near-ultraviolet and visible experimental and calculated spectra at equilibrium for the moderate-pressure condition.

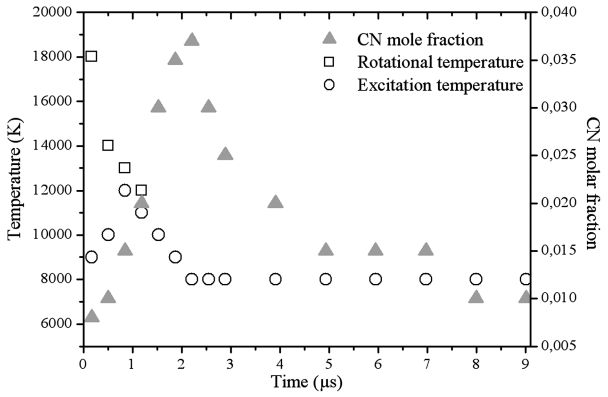

Fig. 8 Evolution of CN mole fraction and temperatures behind the shock front. The experimental conditions are $v_s = 6.9$ km/s, $p_i = 46$ Pa, and $p_s = 2.2 \times 10^4$ Pa. The initial mixture is 70% CO and 30% N_2.

However, those original results include a temporal convolution. In that case, the convolution function can be classed as a Gaussian function with a full width at half-maximum equal to 1.5 μs. The Gaussian shape was determined by using the scattering of a 10 ns pulsed laser. Assuming that the spectral distribution is independent of the temporal convolution, it is easy to rescale the plot of Fig. 8 to obtain evolutions that are directly comparable with kinetic calculations. The result is shown in Fig. 9, which presents the CN molar fraction and temperature temporal profiles along with the theoretical results that will be detailed in Sec. III.C.

Figures 10a and 10b present the deconvoluted temporal profiles of the radiative flux for, respectively, the low- and moderate-pressure conditions. For this last condition, no CN density temporal profile was obtained because of the briefness of the nonequilibrium part, which did not allow a satisfactory signal-to-noise ratio for averaged spectra over 0.13 μs. A comparison of time scales of Figs. 9a and 10a shows that the radiative peak occurs at $t = 0.23$ μs, whereas the molar fraction peak occurs at about $t = 0.35$ s. Moreover, both evolutions are not obviously correlated by the electronic temperature that decreases to reach 8000 K (the equilibrium temperature) when the molar fraction is maximum. The electronic temperature maximum occurs at about $t = 0.13$ μs and is 12,000 K (Fig. 9b). It should be remembered that the time scale origin is not the shock front time, which is not captured. Although the radiative flux is much more sensitive to the electronic temperature than to the CN mole fraction in the case of an excitation by collision from the ground state, an independent kinetics directly yielding the CN($B^2\Sigma^+$) state can not be excluded.

The same analysis was attempted on C_2 Swan spectra but the results were not satisfying, mainly because of the weak self-absorption by those transitions. No distinction is observable between the excitation and rotational temperatures. The temperature decrease behind the shock front is clear but with a very large uncertainty on the temperature in the nonequilibrium part. Otherwise, the equilibrium temperature is also found to be equal to 8000 K.

C. Comparison with Chemical Kinetic and Radiative Calculations

The chemical kinetic calculation was initialized using the perfect gas shock jump conditions (Rankine–Hugoniot equations) and assuming that the thermochemical state of the gas is frozen through the shock. From these new values of pressure, temperature, density, and velocity of the mixture just behind the shock, the downstream flowfield was then computed by temporally solving the one-dimensional Euler equations. The calculation used a two-temperature model in which the electronic excitation is in equilibrium with vibration on the one hand and translation in equilibrium with rotation on the other hand. A detailed description of the implemented physical models is given in [13]. Different chemical models were tested by Park et al. [21], Gökçen [22], and Lee et al. [16], and are hereafter referred to as Park, Gökçen, and Lee for simplicity. The outputs of the chemical kinetic code (temperatures and densities) were then used as inputs for the radiation code PASTIS to derive temporal profiles of the radiative flux.

Equilibrium calculations are in very good agreement with experiments, as shown in Figs. 7 and 11. Unfortunately, the equilibrium is not reached experimentally for the low-pressure condition because of the arrival of the contact surface. Conversely, none of the three models is able to correctly describe the CN violet emission in the nonequilibrium part just behind the shock front. Several reasons can explain such differences: inconvenient chemical kinetics constants (however well-reproduced CN density and temperatures), a bad description of postshock conditions by the Rankine–Hugoniot conservation equations, or an inconvenient physical model. The Park model yields the highest radiative flux, whereas the Gökçen model gives the lowest one. For the moderate-pressure condition,

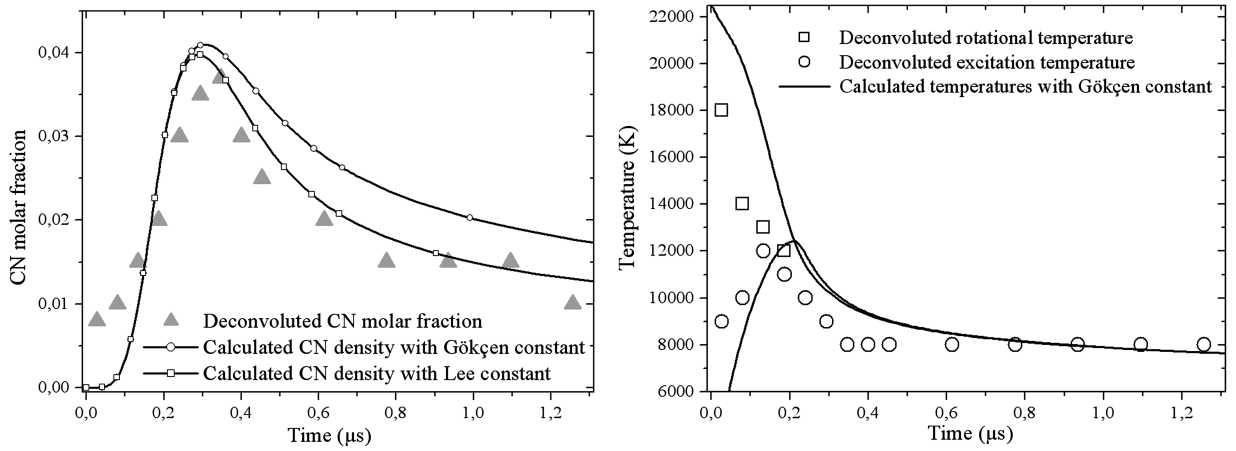

Fig. 9 Deconvoluted temporal profiles for the low-pressure condition: a) CN molar fraction, and b) temperatures.

calculations overestimate the radiative flux by a ratio that varies from 2.0 (Gökçen) to 2.5 (Park). For the low-pressure condition, calculations underestimate the radiative flux by a ratio that varies from 1.2 (Park) to 1.4 (Gökçen).

Those differences between the two-temperature calculations and experimental results are not always observed. For example, calculations carried out to reproduce results from Grinstead et al. [10] with a lower pressure (13.3 Pa) and a higher velocity (8.5 km/s) provided a better agreement with experiments [23] whatever the chemical model.

Moreover, the experimental deconvoluted temporal profiles obtained within this work were compared with the direct results of the chemical kinetic calculations. The calculations were carried out with the Gökçen chemical model but also with the same model with a modification of the reaction rate constant A of the dissociation reaction $C_2 + M \rightarrow C + C + M$ (M being any collider) as proposed by Lee et al. [16].

The forward reaction rate k_f is written using an Arrhenius form:

$$k_f = AT_a^n \exp(-T_d/T_a)$$

where T_a is the geometrical average of kinetic and vibrational temperatures, n is equal to 0, and the activation temperature T_d is equal to 71,600 K. This value was derived from the activation energy measured by Kruse and Roth [24] and is equal to 6.2 ± 0.2 eV. Gökçen proposed that a reaction rate constant A is equal to 2.49×10^{-14} m^3/s [22], whereas Lee et al. fixed it at 1.25×10^{-13} m^3/s [16]. This reaction is crucial for CN formation because it feeds the neutral exchange reaction $N_2 + C \rightarrow CN + N$ as well as the three-body recombination $C + N + M \rightarrow CN + M$. The comparisons between the deconvoluted data and calculations are shown in Figs. 9a and 9b. Experiments and calculations are in rather good agreement for temperatures (Fig. 9b), especially when the rotational and electronic temperatures are close. There are very few differences between both calculations and only the calculation with the constant given by Gökçen is plotted. The equilibrium temperature with the constant proposed by Lee et al. is about 500 K lower (the difference should be ascribed to the way the nonequilibrium rates are deduced through the microreversibility). Of course, the calculation of the CN density evolution is more sensitive to that reaction constant (Fig. 9a). The peak density is quite similar for the experiment and calculations, whereas the CN density decrease is faster experimentally than theoretically. However, the new reaction rate proposed by Lee et al. seems to improve the prediction of CN temporal profiles. These conclusions make sense within the limitations of the mentioned uncertainties on experimental temperatures and densities.

Anyway, in spite of selective successes, two-temperature models do not prove to be convenient to reproduce the nonequilibrium radiation of CN in all cases. Conversely, they seem to be sufficient for chemical kinetics predictions because they correctly reproduce temperatures and densities. The way the CN($B^2\Sigma^+$)) state is produced then has to be addressed and, more generally, the kinetics of electronic excited states has to be taken into account to get accurate predictions of nonequilibrium radiative heat flux. Acquisition with a

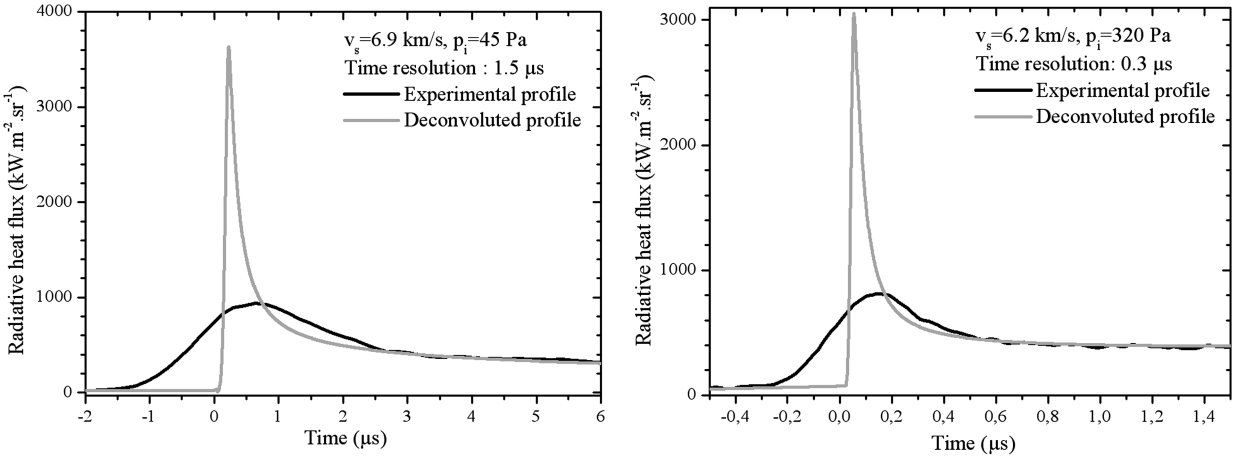

Fig. 10 Deconvoluted temporal profiles: a) low-pressure conditions, and b) moderate-pressure conditions. Note that temporal resolutions and time scales are not the same.

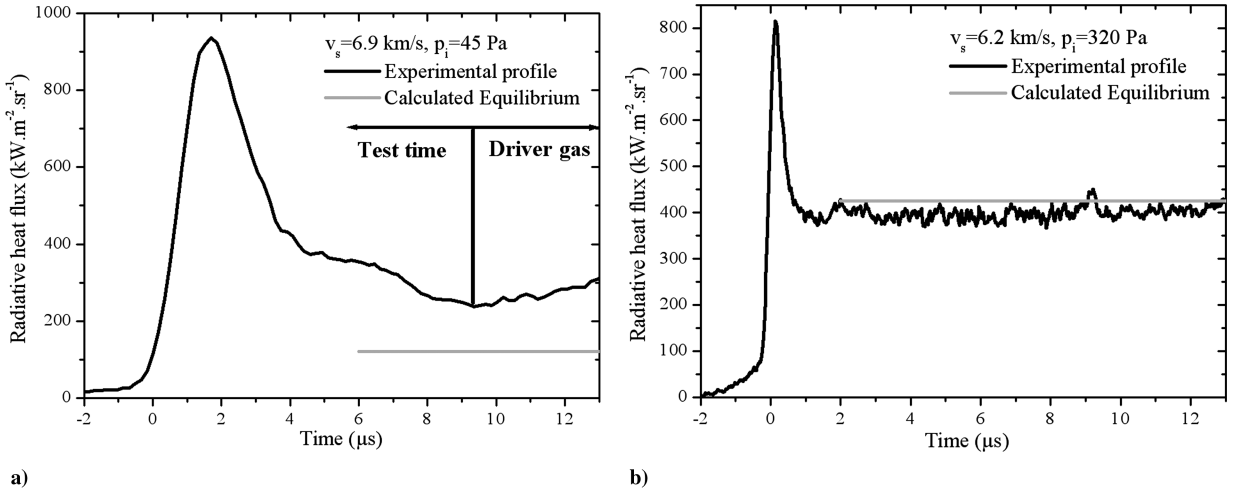

Fig. 11 Experimental temporal profiles of CN violet emission: a) low-pressure conditions, and b) moderate-pressure conditions. In both cases, the initial mixture is 70% CO and 30% N_2. The spectral radiances were integrated over the range of 370–430 nm.

better temporal resolution should bring more accurate data about the nonequilibrium radiative flux.

IV. Results for C_2: CO–N_2 and CO_2–N_2 Mixtures and Pure CO_2

To get some data about the influence of the mixture composition on the radiative flux, further experiments were carried out for the low-pressure condition. The purpose was to point out what the influence of CO_2 dissociation is on the radiative flux. Two other compositions were tested: 70% CO_2–30% N_2 and pure CO_2. Because comparisons could not be made about the CN radiation (there is no CN radiation from a pure CO_2 plasma), the C_2 Swan $\Delta v = +1$ (460–475 nm) manifold was recorded for both new mixture compositions and compared with results obtained for CO–N_2. Similar measurements made on the C_2 Swan $\Delta v = 0$ (480–540 nm) manifold confirmed the following results.

The relaxation of C_2 emission behind the shock wave is expected to be different with regard to the postshock conditions, the temperature evolutions, and the composition. Indeed, the dissociation of carbon dioxide produces a significant amount of oxygen atoms that are not present in such a high concentration in plasmas produced from CO mixtures. Atomic oxygen is expected to efficiently destroy C_2 through the reaction $C_2 + O \rightarrow CO + C$. That reaction should lead to a faster decrease of C_2 emission in plasmas produced from CO_2 mixtures. As mentioned earlier, simple two-temperature calculations were also carried out to predict density and temperature temporal profiles. The results were taken as input in the radiation code PASTIS, and the calculated emission temporal profile for the three mixtures are presented in Fig. 12 with a normalized scale.

The plot in Fig. 12 clearly shows that C_2 relaxation is much faster for the CO_2 mixtures than for the CO mixture, for which the characteristic relaxation time is about 1 μs versus 0.1 μs for pure CO_2. Figure 13b shows the same calculations as in Fig. 12 but includes a convolution that takes into account the temporal resolution (1.5 μs). These simulations may now be compared with the experimental temporal profiles in Fig. 13a. Because of the low temporal resolution, only qualitative conclusions can be drawn from Figs. 13a and 13b. The comparison of characteristic times shows that experimental ones are lower than calculated ones and even much lower in the case of pure CO_2. The calculation does not take into account the specific quenching of excited electronic states. The difference may also be ascribed to incorrect rate coefficients in the model in the case of a production of the excited state by collisional excitation from the ground state. Nevertheless, as the experimental evolutions represent those of the C_2 excited electronic state $d^3\Pi_g$ and not of the C_2 total density, the difference must rather be sought in a specific kinetics of the C_2 excited electronic state $d^3\Pi_g$.

As shown in Fig. 14a, C_2 radiation is one order of magnitude lower for CO_2 mixtures than for the CO mixture. This is an expected result: a significant part of the shock energy being used in CO_2 dissociation, atoms and radicals responsible for C_2 formation are present in lower concentration in the plasma. In the same way, C_2 Swan emission is slightly higher for pure CO_2 than for a mixture containing 70% CO_2. The calculations presented in the preceding paragraph are also presented in Fig. 14b with an absolute logarithmic scale. A comparison between Figs. 14a and 14b shows that, in all cases, experimental values are about four times higher than calculated ones, including for longer times (even if equilibrium is not reached during the experiment, the value of the radiative flux can be estimated to be higher than that predicted). Using different sets of reaction rates, the ratio varies from 2.5 (Park) to 5 (Gökçen). The difference may be clearly ascribed to the reactions included in the model that lead only to the formation of C_2 in its ground state, followed by collisional excitation to the upper state of the C_2 Swan system at a temperature fixed to a common vibrational temperature. The recorded emission from C_2 is rather a chemiluminescence, which means that C_2 is directly produced in the electronic excited state.

This is a critical limitation of two-temperature and multitemperature models: they are not able to correctly deal with the kinetics of excited states. Some evolutions were recently proposed by taking into account precursor phenomena and using an improved translation–vibration exchange model [25]. Some others authors proposed an independent calculation of the electronic excitation

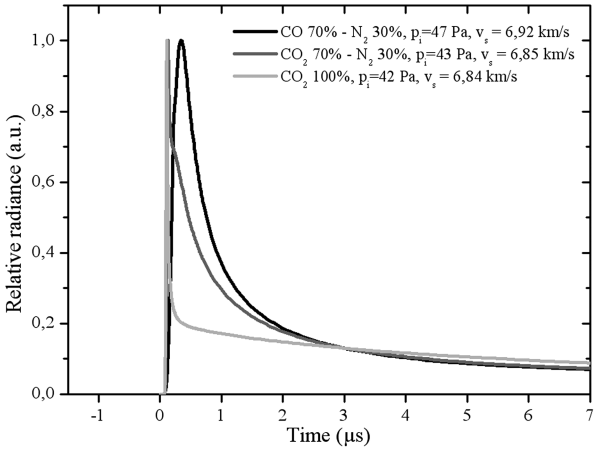

Fig. 12 Calculation of the temporal profile of C_2 Swan $\Delta v = +1$ normalized emission for three different mixtures and similar pressure and shock velocity conditions. The spectral radiances were integrated over the range of 460–475 nm.

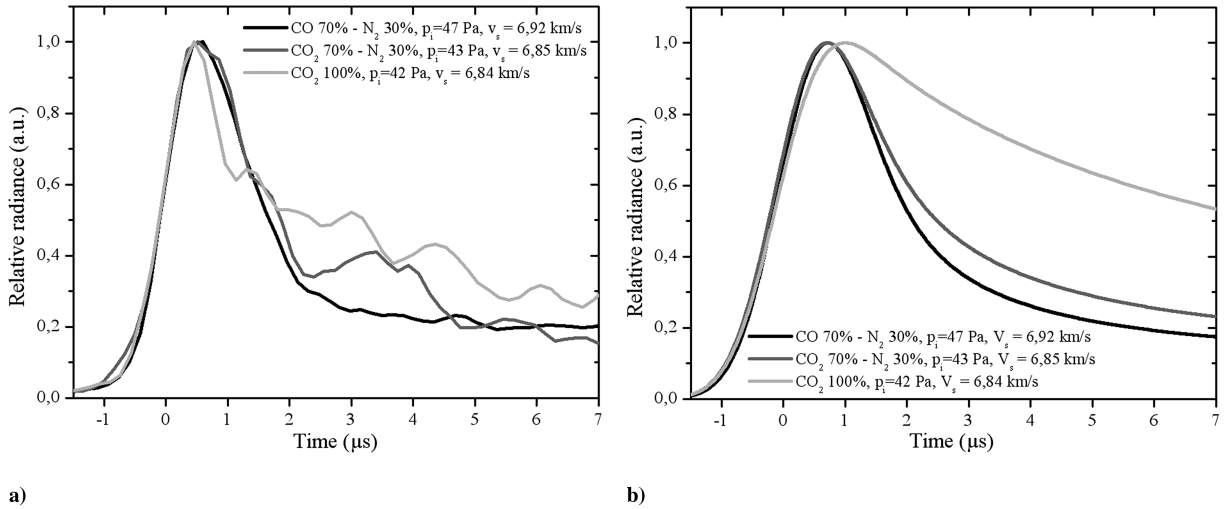

a) b)

Fig. 13 Temporal profile of C_2 Swan $\Delta v = +1$ normalized emission for three different mixtures and similar pressure and shock velocity conditions: a) experimental, and b) calculated then convoluted.

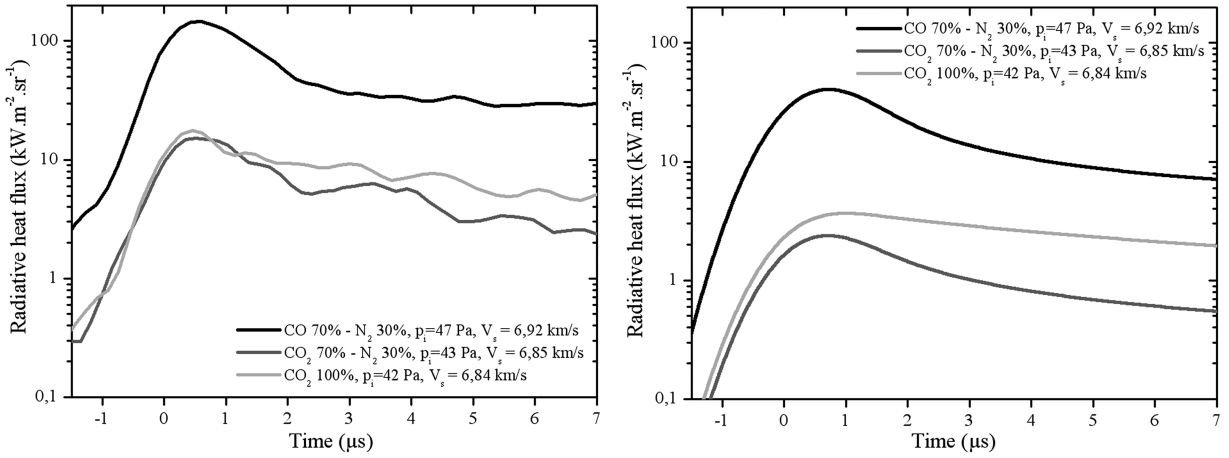

a) b)

Fig. 14 Temporal profile of C_2 Swan $\Delta v = +1$ absolute emission for three different mixtures and similar pressure and shock velocity conditions: a) experimental, and b) calculated then convoluted.

with, moreover, a loose coupling of radiation, chemistry, and flowfield [26]. Those new models bring important improvements in the comparison between shock-tube experiments and calculated results. For example, the delay appearing in electronic temperature evolutions with regard to vibrational temperature evolutions [26] leads to a CN radiative flux density closer to experimental results and should allow one to conclude whether the $CN(B^2\Sigma^+)$ state is produced by collisional excitation from the ground state or through the chemistry. However, the simple shock-tube geometry should encourage the development of an electronic state-to-state model that could be validated with a reasonable computation time cost.

V. Conclusions

Experimental results concerning the radiation behind a strong shock wave in Martian-like mixtures are presented. They were obtained in a moving shock tube using an original afocal optical setup without using any fiber optics. This system allows an increase in the amount of collected light and a drastic improvement in the reproducibility. Time-spectral images of the CN violet radiation were postprocessed to derive radiative flux temporal profiles. The comparison of those evolutions with the results of a radiation code taking into account self-absorption provided the temperature and molar fraction temporal profiles. The determination of density evolutions is a great step that could be improved with a better temporal resolution of the acquisition channel. It should be possible to get a resolution close to the limit imposed by the shock front curvature. Such an improvement should go with an accurate determination of the shock time that could give the incubation times of excited CN and C_2 formation. Those values are of a great interest for the validation of chemical and physical models. The comparison of the results obtained with different mixtures shows that the dissociation of carbon dioxide significantly influences the C_2 radiative flux as well as the relaxation of C_2 emission because of released atomic oxygen. More experiments with various amount of CO_2 and perhaps mixtures of CO_2 and CO should bring complementary data on CO_2 dissociation, especially if CO vibrational excitation is tracked. Following the way opened by the recent measurements at the NASA Ames Research Center, vacuum ultraviolet radiation, especially from the fourth positive system of CO, has to be addressed.

A general comparison of experiments with a simple two-temperature calculation proves that experiments need more complex modelling, such as a collisional-radiative model to be correctly rebuilt in the nonequilibrium phase. If it gives very important and direct information on the energy load of a space vehicle during a Martian entry, the measurement of the radiative flux is an indirect way to study chemical kinetics processes. Many questions remain on chemical reaction modeling, especially on dissociation and more especially on carbon dioxide dissociation. The issue of excited state formation should also be addressed, and measurements of

ground-state densities as well as excited-state densities will help to reach that purpose. When possible, the use of self-absorption is shown to be a good opportunity. Nevertheless, the validation of existing models needs more experimental data, especially in shock tubes. Other experimental techniques such as diode-laser absorption spectroscopy and laser-induced fluorescence should be more widely used in the future.

Acknowledgments

The authors express sincere thanks to Jean-Marie Félio for his help in conducting some of the experiments and to Stéphane Martinez for the design and making of the shock velocity measurement device. The authors are also grateful to Arnaud Bultel, Bruno G. Chéron, Julien Jarrige, and Pierre Vervisch for their careful reading and useful comments. Pascal Boubert also acknowledges support of this research by the Institut Universitaire des Systèmes Thermiques Industriels at the University of Provence in Marseille, France.

References

[1] Laub, B., and Venkatapathy, E., "Thermal Protection System Technology and Facility Needs for Demanding Future Planetary Missions," *Proceedings of the International Workshop on Planetary Probe Atmospheric Entry and Descent Trajectory Analysis and Science*, SP-544, ESA, Paris, 2006, pp. 239–247.

[2] Boubert, P., and Vervisch, P., "CN Spectroscopy and Physico-Chemistry in the Boundary Layer of a C/SiC Tile in a Low Pressure Nitrogen/Carbon Dioxide Plasma Flow," *Journal of Chemical Physics*, Vol. 112, No. 23, 2000, pp. 10482–10490. doi:10.1063/1.481682

[3] Studer, D., and Vervsch, P., "Raman Scattering Measurements Within a Flat Plate Boundary Layer in an Inductively Coupled Plasma Wind Tunnel," *Journal of Applied Physics*, Vol. 102, No. 3, 2007, p. 033303. doi:10.1063/1.2768067

[4] Nealy, J. E., and Haggard, K. V., "A Shock Tube Study of Radiation Behind Shock Waves in CO_2 with Application to Venus Entry," *Proceedings of the 9th International Symposium on Shock Tubes and Waves*, edited by D. Bershader, and W. Griffith, Stanford Univ. Press, Palo Alto, CA, 1973, pp. 330–339.

[5] Nealy, J. E., "An Experimental Study of Ultraviolet Radiation Behind Incident Normal Shock Waves in CO_2 at Venusian Entry Speeds," AIAA Paper 75-1150, 1975.

[6] Thomas, G. M., and Menard, W. A., "Experimental Measurements of Nonequilibrium and Equilibrium Radiation from Planetary Atmospheres," *AIAA Journal*, Vol. 4, No. 2, 1966, pp. 227–237. doi:10.2514/3.3423

[7] Gorelov, V. A., Gladyshev, M. K., Kireev, A. Y., Tchebureev, V. G., and Shilenkov, S. V., "Nonequilibrium Ionization and Radiation Behind Shock Wave in Martian Atmosphere," *Proceedings of the 3rd European Symposium on Aerodynamics for Space Vehicles*, SP-426, ESA, Paris, 1998, pp. 429–436.

[8] Losev, S. A., Kozlov, P. V., Kuznetsova, L. A., Makarov, V. N., Romanenko, Y. V., Surzhikov, S. T., and Zalogin, G. N., "Radiation of a Mixture CO_2–N_2–Ar in Shock Waves: Experiment and Modelling," *Proceedings of the 3rd European Symposium on Aerodynamics for Space Vehicles*, SP-426, ESA, Paris, 1998, pp. 437–444.

[9] Bose, D., Wright, M. J., Bogdanoff, D. W., Raiche, G. A., and Allen, G. A., "Modeling and Experimental Assessment of CN Radiation Behind a Strong Shock Wave," *Journal of Thermophysics and Heat Transfer*, Vol. 20, No. 2, 2006, pp. 220–230. doi:10.2514/1.16869

[10] Grinstead, J. H., Wright, M. J., Bogdanoff, D. W., and Allen, G. A., "Shock Radiation Measurements for Mars Aerocapture Radiative Heating Analysis," *Journal of Thermophysics and Heat Transfer*, Vol. 23, No. 2, 2009, pp. 249–255. doi:10.2514/1.37281

[11] Bose, D., Grinstead, J. H., Bogdanoff, D. W., and Wright, M. J., "Shock Layer Radiation Measurements and Analysis for Mars Entry," *Proceedings of the 3rd International Workshop on Radiation of High Temperature Gases in Atmospheric Entry*, SP-667, ESA, Paris, 2009.

[12] Rond, C., Boubert, P., Félio, J. M., and Chikhaoui, A., "Radiation Measurements in a Shock Tube for Titan Mixtures," *Journal of Thermophysics and Heat Transfer*, Vol. 21, No. 3, 2007, pp. 638–646. doi:10.2514/1.28422

[13] Rond, C., Boubert, P., Félio, J. M., and Chikhaoui, A., "Nonequilibrium Radiation Behind a Strong Shock Wave in CO_2–N_2," *Chemical Physics*, Vol. 340, Nos. 1–3, 2007, pp. 93–104. doi:10.1016/j.chemphys.2007.08.003

[14] Anokhin, E. M., Ivanova, T. Y., Kudryatsev, N. N., and Starikovskii, A. Y., "Dynamics of Radiation in a CO:N_2 Mixture Behind Strong Shock Waves," *High Temperature*, Vol. 45, No. 6, 2007, pp. 733–739. doi:10.1134/S0018151X07060028

[15] Anohin, E. M., Ivanova, T. Y., Koudriavtsev, N. N., and Starikovskii, A. Y., "Non-Equilibrium Radiation and Physical–Chemical Processes in Martian Atmosphere in Strong Shock Waves," AIAA Paper 05-792, 2005.

[16] Lee, E. S., Park, C., and Chang, K. S., "Shock-Tube Determination of CN Formation Rate in a CO–N_2 Mixture," *Journal of Thermophysics and Heat Transfer*, Vol. 21, No. 1, 2007, pp. 50–56. doi:10.2514/1.25144

[17] Brandis, A., McIntyre, T., Morgan, R., and Jacobs, P., "Overview of Radiation Intensity Measurements on the X2 Facility at the University of Queensland," *Proceedings of the 3rd International Workshop on Radiation of High Temperature Gases in Atmospheric Entry*, SP-667, ESA, Paris, 2009; also Brandis, A. M., Morgan, R. G., McIntyre, T. J., and Jacobs, P. A., "Nonequilibrium Radiation Intensity Measurements in Simulated Titan Atmospheres," *Journal of Thermophysics and Heat Transfer* (to be published).

[18] Labracherie, L., Dumitrescu, M. P., Burtshell, Y., and Houas, L., "On the Compression Process in a Free-Piston Shock Tunnel," *Shock Waves*, Vol. 3, No. 1, 1993, pp. 19–23. doi:10.1007/BF01414744

[19] Boubert, P., Chaix, A., Chikhaoui, A., Robin, L., and Vervisch, P., "Aerodynamic Calibration of TCM2 Facility and Study of a Bow Shock Layer by Emission and Laser Spectroscopy," *Shock Waves*, Vol. 11, No. 5, 2002, pp. 341–351. doi:10.1007/s001930100117

[20] Rond, C., "Etude Expérimentale et Numérique de la Cinétique Chimique et Radiative hors d'Équilibre à l'Aval d'une Onde de Choc Stationnaire. Application aux Entrées Atmosphériques de Mars et Titan," Ph.D. Thesis, University of Provence, Marseille, France, 2006.

[21] Park, C., Howe, J. T., Jaffe, R. L., and Candler, G. V., "Review of Chemical-Kinetic Problems of Future NASA Missions, II: Mars Entries," *Journal of Thermophysics and Heat Transfer*, Vol. 8, No. 1, 1994, pp. 9–23. doi:10.2514/3.496

[22] Gökcen, T., "N_2–CH_4–Ar Chemical Kinetic Model for Simulations of Titan Atmospheric Entry," *Journal of Thermophysics and Heat Transfer*, Vol. 21, No. 1, 2007, pp. 9–18. doi:10.2514/1.22095

[23] Boubert, P., and Rond, C., "Radiation behind a strong shock wave in Martian-like mixtures," *Proceedings of the 3rd International Workshop on Radiation of High Temperature Gases in Atmospheric Entry*, SP-667, ESA, Paris, 2009.

[24] Kruse, T., and Roth, P., "Kinetics of C2 Reactions During High-Temperature Pyrolysis of Acetylene," *Journal of Physical Chemistry A*, Vol. 101, No. 11, 1997, pp. 2138–2146. doi:10.1021/jp963373o

[25] Hyun, S. Y., Park, C., and Chang, K. S., "Rate Parameters for Electronic Excitation of Diatomic Molecules: CN Radiation," *Journal of Thermophysics and Heat Transfer*, Vol. 23, No. 2, 2009, pp. 226–235. doi:10.2514/1.36749

[26] Potter, D. F., Gollan, R. J., Jacobs, P. A., and Leyland, P., "Numerical Simulations and Analysis of the 8.5 km/s CO_2–N_2 EAST Shock Tube Condition," *Proceedings of the 3rd International Workshop on Radiation of High Temperature Gases in Atmospheric Entry*, SP-667, ESA, 2009.

[27] Braun, R. D., and Manning, R. M., "Mars Exploration Entry, Descent, and Landing Challenges," *Journal of Spacecraft and Rockets*, Vol. 44, No. 2, 2007, pp. 310–323. doi:10.2514/1.25116